A study of the NO_x dependence of isoprene oxidation

Dennis J. Barket Jr.,[1,2] John W. Grossenbacher,[1,2] Julia M. Hurst,[1] Paul B. Shepson,[1,3] Kenneth Olszyna,[4] Troy Thornberry,[5] Mary Anne Carroll,[5,6] James Roberts,[7] Craig Stroud,[7] Jan Bottenheim,[8] and Thomas Biesenthal[9]

Received 9 July 2003; revised 11 February 2004; accepted 2 March 2004; published 15 June 2004.

[1] A large set of isoprene and isoprene oxidation product concentration data from four North American sites was examined to assess the NO_x dependence of the daytime oxidation of isoprene. Sites that represent a wide range of NO_x (50 ppt to 30 ppb) were studied and include the Dickson, Tennessee, and Cornelia Fort Air Park sites during the 1999 Southern Oxidants Study, the Pellston, Michigan, site during the 1998 PROPHET summer intensive, and the Kejimkujik National Park site during the Atlantic 1996 study. Knowledge of NO_x and HO_x concentrations were critical for this evaluation. While NO_x data are readily available at all sites, HO_x data are limited. We employed a simple 10-reaction HO_x model to calculate steady state OH radical concentrations as a function of [NO_x] to enable analysis of the data from all sites. Here, we use methyl vinyl ketone (MVK) concentrations to quantify the extent of isoprene-OH oxidation. Making use of the MVK/isoprene ratio, we show that the rate of production of isoprene oxidation products at various North American sites, although highly variable, exhibits the crossover from NO_x-dependent to VOC-dependent conditions at ~8 ppb [NO_x], in agreement with what is calculated from HO_x measurements and our calculations. *INDEX TERMS:* 0315 Atmospheric Composition and Structure: Biosphere/atmosphere interactions; 0345 Atmospheric Composition and Structure: Pollution—urban and regional (0305); 0365 Atmospheric Composition and Structure: Troposphere—composition and chemistry; *KEYWORDS:* isoprene nitrates, nitrogen oxides, isoprene

Citation: Barket, D. J., Jr., et al. (2004), A study of the NO_x dependence of isoprene oxidation, *J. Geophys. Res.*, *109*, D11310, doi:10.1029/2003JD003965.

1. Introduction

[2] The role of biogenic volatile organic compounds (BVOCs) in tropospheric chemistry processes, including the formation of ground level ozone, is well documented [*Trainer et al.*, 1987; *Chameides et al.*, 1992; *Biesenthal et al.*, 1997]. One molecule, isoprene (2-methyl-1, 3-butadiene), is a particularly significant BVOC, as it accounts for ~44% of the total nonmethane VOC global emissions [*Guenther et al.*, 1995], and is very reactive. Isoprene's abundance and reactivity cause it to dominate boundary layer tropospheric chemistry in most forested regions [*Trainer et al.*, 1987] and even some urban environments [*Chameides et al.*, 1988; *Biesenthal et al.*, 1997]. Furthermore, in isoprene-impacted environments, the isoprene oxidation products methyl vinyl ketone, methacrolein, and formaldehyde can also be important O_3 precursors [*Cantrell et al.*, 1993; *Starn et al.*, 1998; *Sumner et al.*, 2001; *Stroud et al.*, 2001]. Although it is well known that isoprene can be the dominant reactive VOC during summer in eastern North America [*Chameides et al.*, 1992], the extent to which isoprene chemistry contributes to ozone production is highly dependent on NO and NO_2 (NO_x) concentrations. The NO_x dependence of BVOC-related ozone production chemistry will be partly reflected in the concentrations of the isoprene oxidation products, which may be used as a surrogate measure of isoprene's role in ozone formation [*Biesenthal et al.*, 1997]. Although this can be examined with computer models, the NO_x dependence of isoprene chemistry has yet to be tested with field observations of isoprene and its oxidation products. To this end, field data from four ground sites have been assembled and analyzed. The sponsoring studies and field sites are the 1999 Southern Oxidants Study with sites at Dickson, Tennessee, and Nashville, Tennessee (Cornelia Fort Air Park); PROPHET 1998 at Pellston, Michigan; and the ATLANTIC 96 study at Kejimkujik National Park, Nova Scotia. At these sites, ozone, isoprene, methyl vinyl ketone (MVK), methacrolein (MACR), HCHO, NO, NO_2, and

[1]Department of Chemistry, Purdue University, West Lafayette, Indiana, USA.
[2]Now at Griffin Analytical Technologies, Inc., West Lafayette, Indiana, USA.
[3]Department of Earth and Atmospheric Sciences, Purdue University, West Lafayette, Indiana, USA.
[4]Atmospheric Sciences Department, Tennessee Valley Authority, Muscle Shoals, Alabama, USA.
[5]Department of Atmospheric, Oceanic, and Space Sciences, University of Michigan, Ann Arbor, Michigan, USA.
[6]Department of Chemistry, University of Michigan, Ann Arbor, Michigan, USA.
[7]NOAA Aeronomy Laboratory, Boulder, Colorado, USA.
[8]Meteorological Service of Canada, Downsview, Ontario, Canada.
[9]Sciex, Mississauga, Ontario, Canada.

Copyright 2004 by the American Geophysical Union.
0148-0227/04/2003JD003965

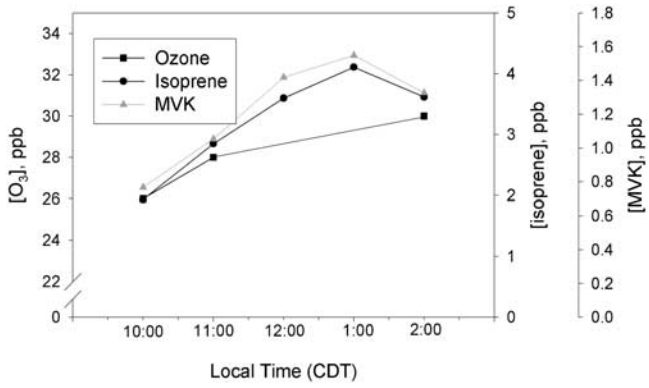

Figure 1. Observed ozone, isoprene, and MVK data for 1 July 1999, Dickson, Tennessee.

meteorological parameters were measured during the summer months.

1.1. OH-Isoprene Oxidation

[3] Using the fact that the reaction of OH with isoprene produces organic peroxy radicals that then react to produce both O_3 and carbonyl compounds, we can estimate the contribution of isoprene to local ozone production [*Biesenthal et al.*, 1997]. Isoprene reaction with OH can involve the addition of OH to any of the four carbons associated with the isoprene double bonds [*Stevens et al.*, 1999; *Lei et al.*, 2001]. The subsequent addition of O_2 to the carbon-centered alkyl radical produces an organic peroxy radical (RO_2), as shown in reaction (R1). The RO_2 radicals can proceed through several reaction channels, which are presented in reactions (R2a), (R2b), (R3), and (R4). In reactions (R2a) and (R6), NO is oxidized to NO_2. Each time an NO_2 is generated in a sunlit environment, it will lead to an ozone molecule; therefore, under certain atmospheric conditions (sunlit, high NO_x), ~2 ozone molecules can be generated from each OH oxidation of an isoprene molecule (or other VOC).

(R1) $OH + Isoprene(+O_2) \rightarrow RO_2$

(R2a) $RO_2 + NO \rightarrow RO + NO_2$

(R2b) $RO_2 + NO \rightarrow RONO_2$

(R3) $RO_2 + HO_2 \rightarrow ROOH + O_2$

(R4) $RO_2 + RO_2 \rightarrow 2RO + O_2$

(R5) $RO + O_2 \rightarrow carbonyls + HO_2$

(R6) $HO_2 + NO \rightarrow NO_2 + OH$

(R7) $OH + NO_2 \rightarrow HNO_3$

[4] As discussed in detail by *Biesenthal et al.* [1997], an expression can be derived for the contribution of isoprene oxidation to local ozone production, making use of the fact that MVK is produced at a known yield, as O_3 is produced from isoprene oxidation. From the data presented by *Chen et al.* [1998] regarding isoprene nitrate yields (i.e., k_{2a}/k_2 = 0.956, and thus each time isoprene is oxidized, 2×0.956 = 1.91 O_3 molecules are produced), and that at high [NO_x], the MVK yield is 0.32 [*Tuazon and Atkinson*, 1990; *Miyoshi et al.*, 1994], we can derive equation (1). Equation (1) can be used to estimate the amount of ozone produced from isoprene-OH oxidation (not including the contribution from secondary oxidation of the isoprene oxidation products), per molecule of the product MVK.

$$\frac{P(O_3 \text{ from Isoprene})}{P(MVK)} = \frac{1.91R1}{0.32R1} = 6.0 \quad (1)$$

[5] In Figure 1, ozone, isoprene, and MVK data from 1 July 1999 at Dickson, Tennessee, are presented. The time frame was chosen so that the breakup of the nocturnal boundary layer had occurred or largely occurred and there was thorough mixing in the boundary layer. Also, for the assumption to be valid, MVK production must be greater than MVK loss, which is generally the case for daytime boundary layer conditions [*Biesenthal et al.*, 1998]. For [isoprene] = 3 ppb, and [MVK] = 1 ppb, the loss of MVK via OH reaction is only 18% of the rate of MVK production. Because MVK is a stable isoprene-OH reaction product and the daytime MVK rate of production dominates its rate of destruction, the measurement of MVK provides an opportunity to evaluate the daytime isoprene oxidation rate and its contribution to ozone production.

[6] For this day the change in ozone was 4.0 ppb from t = 1000 to 1400 local time, and the change in MVK was 0.56 ppb for the corresponding time. The actual change in ozone of course represents the difference between photochemical production and the sum of all loss processes. In the boundary layer, ozone loss will be dominated by dry deposition. If we assume a deposition velocity for daytime conditions in forest environments as 1.0 cm/s [*Padro*, 1996], and a boundary layer height of 1000 m, then we calculate a first-order loss rate constant of 1×10^{-5} s^{-1}. For 30 ppb O_3, this corresponds to a loss of 4.3 ppb over this 4-hour period. Thus if this is the dominant loss mechanism, the total production of O_3 was 10.3 ppb. Then from equation (1), and these data, we calculate that $4.0 \cdot (0.56/10.3) = 0.22$, or ~22% of the ozone produced during this time was derived from isoprene oxidation. This calculation assumes a homogeneous air mass, and that all RO_2 radicals react with NO.

[7] While this type of analysis is useful, it is limited in its scope and does not allow for a comprehensive understanding of isoprene chemistry covering a wide range of NO_x concentrations. To date, several models have investigated the NO_x dependence of atmospheric OH-VOC chemistry [*Lin et al.*, 1988; *Chameides et al.*, 1992; *McKeen et al.*, 1997; *Frost et al.*, 1998]. However, the NO_x dependence has not been explicitly examined through observation of isoprene oxidation products. Such a tool is useful, as products such as MVK are much easier to quantify in the field than is [OH], and this provides a means to assess the

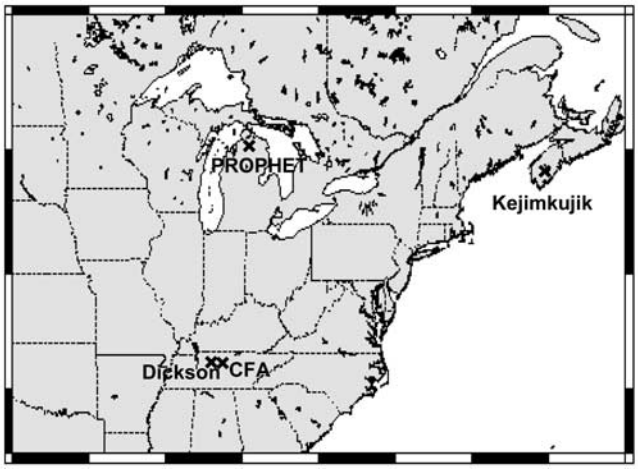

Figure 2. Map of the field site locations.

extent to which an environment is NO_x or VOC limited with respect to ozone production.

1.2. NO_x Dependence of Isoprene-OH Oxidation

[8] Part of the expected NO_x dependence of the isoprene chemistry arises from the NO_x dependence of HO_x radical concentrations [*Lin et al.*, 1988; *Cantrell et al.*, 1992]. Peroxy radicals are produced via OH reaction with volatile organic compounds (VOCs), but their fate (and thus concentration) depends on NO_x in a nonlinear way. At low [NO_x], peroxy radicals terminate via self-reaction and reaction with HO_2, as shown in reactions (R3) and (R4). At high [NO_x], OH is consumed by the reaction with NO_2 to form nitric acid, as shown in reaction (R7). Thus the HO_x radical concentration depends nonlinearly on [NO_x].

[9] A potential limitation of the analysis presented in section 1.1 is the assumption that all of the peroxy radicals react with NO. We can treat the other peroxy radical reaction channels by introducing the variable γ, where γ = the fraction of the time RO_2 reacts with NO versus HO_2 and RO_2. The quantity γ is calculated as follows:

$$\gamma = \frac{(k_2[RO_2][NO])}{(k_2[RO_2][NO] + k_3[RO_2][HO_2] + k_4[RO_2][RO_2])} \quad (2)$$

[10] The associated rate constants for calculation of γ are 9.0×10^{-12} cm^3/molecules·s for RO_2 + NO (i.e., for the isoprene peroxy radicals) [*Stevens et al.*, 1999], 3.9×10^{-12} cm^3/molecules·s for RO_2 + RO_2 [*Jenkin et al.*, 1998], and 1.3×10^{-11} cm^3/molecules·s for RO_2 + HO_2 [*Kirchner and Stockwell*, 1996].

[11] As discussed above, [MVK] can be used to evaluate daytime isoprene oxidation chemistry. The production rate, P, for MVK is given in equation (3),

$$P[MVK] = k_1[OH][isoprene]\{(\gamma \cdot \alpha) + (1 - \gamma) \cdot \beta\} \quad (3)$$

where α represents the experimental yield of MVK from isoprene-OH oxidation in high-NO_x conditions and β represents the experimental yield of MVK in low-NO_x conditions. Experimental results have shown that $\alpha = 0.32$ [*Tuazon and Atkinson*, 1990] and $\beta = 0.17$ [*Miyoshi et al.*, 1994]. At high NO_x, some of the peroxy radicals react with NO leading to an alkoxy radical, which decomposes to yield MVK, with a 32% yield. In low-NO_x conditions, the peroxy radical will react with HO_2 and organic peroxy radicals, resulting in the lower 17% MVK yield [*Miyoshi et al.*, 1994].

[12] If we divide both sides of equation (3) by [isoprene], as shown in equation (4), it is evident that the [isoprene] normalized MVK production rate is dependent on two variables: [OH] and γ. Thus we predict that the ratio of atmospheric [MVK]/[isoprene] has a NO_x dependence that mimics that of the NO_x dependence for the quantity [OH] · $\{\gamma \cdot \alpha + (1 - \gamma) \cdot \beta\}$.

$$\frac{P[MVK]}{[Isoprene]} = k_1[OH]\{(\gamma \cdot \alpha) + (1 - \gamma) \cdot \beta\} \quad (4)$$

[13] According to equation (4), concentrations of NO, NO_2, isoprene, MVK, RO_2 OH, and HO_2 are needed to provide a quantitative treatment of the NO_x dependence of isoprene-OH chemistry. To this end, field data from the four ground sites have been amassed and analyzed. The intensive studies at these four field sites provided high-quality BVOC data and represent a unique opportunity, in that the conditions spanned a wide range of NO_x concentrations (nearly 3 orders of magnitude). Unfortunately, there were no [HO_x] measurements conducted at the Kejimkujik and Dickson sites; also, the PROPHET OH data set was limited because of the lack of time-matched data and/or instrumental down time. Therefore it was necessary to develop a method to estimate the concentrations of OH and HO_2 for all four field sites. A steady state approximation method was implemented to provide the HO_x data necessary to conduct an analysis of isoprene chemistry. The steady state calculation method was employed to enable ready calculation for a large and variable reactant species concentration data set, rather than having to formulate and run a photochemical model simulation for each set of MVK/isoprene data. The details of the HO_x steady state approximation are provided in section 3.

2. Experiment

2.1. Field Sites

[14] The four field sites were chosen because of the range of NO_x levels and the availability of high-quality measurement data for NO_x, O_3, H_2O, isoprene, methyl vinyl ketone (MVK), and radiation from each site. Table 1 provides the average values for temperature, [ozone], [isoprene], and [NO_x] during the field intensives for time-matched data from 1000 to 1600 local time. The 1000–1600 time frame was chosen to minimize the effect of rapidly changing boundary layer heights and to enable us to employ a steady state assumption for HO_x. The locations of the four field sites are shown in Figure 2.

[15] The data set from the Kejimkujik site was produced during the 1996 North American Research Strategy for Tropospheric Ozone Canada East (NARSTO-CE) as described at http://odysseus.owt.com/Narsto/. Kejimkujik National Park is located in southern Nova Scotia, Canada, 150 km WSW of the city of Halifax. This remote site is 131 m above sea level and located at 44°26′N, 65°12′W. The forest surrounding the site is approximately 2/3 conif-

Table 1. Average Values of the Time-Matched Data for Key Variables for the Four Field Sites (1000–1600 Local Time)

	Site			
	Kejimkujik	PROPHET	Dickson	CFA
Study period	18 June to 24 July 1996	11 July to 21 August 1998	15 June to 15 July 1999	15 June to 15 July 1999
NO_x, ppb	0.15	0.50	1.85	6.40
O_3, ppb	32	47	44	66
Isoprene, ppb	1.14	2.90	1.72	0.53
Average temperature, °C	19.7	25.9	25.1	30.5

erous and 1/3 deciduous. Instruments were housed in a mobile laboratory. A more detailed description of the site is given by *Bottenheim et al.* [1994].

[16] The PROPHET field site is located at the University of Michigan Biological Station (UMBS), at Pellston, Michigan (45°32′N, 84°40′W), and 240 m above sea level. UMBS occupies 9000 acres of northern hardwood forest containing mostly aspen and birch with an undergrowth of white pine. The average canopy height is 20 m. The site is 30 km due east of Lake Michigan and 50 km due west of Lake Huron. At the PROPHET site, there is a 31 m walk-up scaffold tower that supports a 5 cm diameter Pyrex glass manifold with an inlet positioned at 34 m. A detailed description of the site and meteorology is given by *Carroll et al.* [2001] and *Cooper et al.* [2001].

[17] Isoprene and its oxidation products were measured during the 1999 Southern Oxidants Study at several locations around the Nashville, Tennessee, area. Data from two of these locations, Dickson, Tennessee, and the Cornelia Fort Air Park, Nashville, Tennessee, were used in this study. The Dickson, Tennessee, site is ~50 km west of downtown Nashville at 36°14′N, 87°21′W and resides at an elevation of 225 m above sea level. The area is predominantly a mix of deciduous trees and pastureland. The sampling station was in a clearing on a small hill. Sampling was conducted through a 10 m Pyrex manifold.

[18] The 1999 Southern Oxidants Study Cornelia Fort Airport site at Nashville, Tennessee is 127 m above sea level and positioned at 36°25′N, 86°59′W. This site is in metropolitan Nashville, approximately 7 km northeast of downtown Nashville. The actual sampling site was in a clearing ~200 m from the Cumberland river. Sampling was conducted from a 10 m tower that included a 12 m Pyrex glass sampling manifold. This site is regularly impacted by flow from downtown Nashville. A more detailed description of the CFA SOS field site is given by *Stroud et al.* [2001].

2.2. Measurement Data

[19] From each site quantitative measurement data for isoprene, MVK, MACR, NO, NO_2, O_3, HCHO, and meteorological data, including temperature, relative humidity, and radiation were used as inputs for the HO_x calculation. Methane and CO were assumed to be 1720 ppb [*Dlugokencky et al.*, 1994] and 150 ppb [*Chin et al.*, 1994], respectively. There is of course variability in CO, but in these environments in the boundary layer, a 150 ppb CO estimate is typical, and CO is a relatively small sink for OH in these summertime boundary layer environments [*Sumner et al.*, 2001; *Hurst et al.*, 2003].

[20] For Kejimkujik, the meteorological, radiation, ozone (TECO Model 49 UV absorption) and NO_x (Ecophysics Model CLD770AL instrument) data were made available by Environment Canada. Isoprene, MVK, and MACR data were collected using an autosampler utilizing a Tenax TA-based preconcentrator built in the Shepson laboratory at York University. Analyte separation and detection was achieved using a HP 5890 Series II GC equipped with a HP 5972A mass selective detector [*Biesenthal et al.*, 1998]. Formaldehyde data were obtained using a mist chamber/DNPH/HPLC method [*Leaitch et al.*, 1999]. Acetaldehyde levels were estimated to be 20% of [formaldehyde], on the basis of observations from other field sites that demonstrate an acetaldehyde to formaldehyde ratio of 0.14–0.26 [*Shepson et al.*, 1991; *Cantrell et al.*, 1992, 1993; *Apel et al.*, 1998].

[21] At PROPHET, meteorological and ozone data were made available by the University of Michigan. NO_x data were produced using an ozone chemiluminescence-based NO_x monitor designed and built at the University of Michigan [*Thornberry et al.*, 2001]. Isoprene concentrations were determined using an autosampler with a Tenax TA preconcentrator in conjunction with a HP 5890 Series II GC and a HP 5972A MSD [*Barket et al.*, 2001] for separation and detection. Formaldehyde was determined using a continuous flow injection method based on the reaction of formaldehyde and cyclohexanedione [*Sumner et al.*, 2001]. OH measurements were carried out using a laser-induced fluorescence method as described by *Faloona et al.* [2001]. Acetaldehyde data were obtained (NCAR) using an online GC/MS method with cryogenic preconcentration [*Barket et al.*, 2001]. When acetaldehyde data were not available, its concentration was estimated at 0.17 · [HCHO], which was determined from the average of the actual time-matched measurement data available from PROPHET.

[22] Meteorological, radiation, ozone, and NO_x data at the Dickson site were produced using the SOS level 2 ground-based air monitoring station. A detailed description of the SOS level 2 station is given by *Olszyna et al.* [1998]. The measurement data, as well as a summary of the sampling techniques, for the Dickson site are given by (K. J. Olszyna, NARSTO SOS99NASH TVA surface meteorology and chemistry data, available online at http://eosweb.larc.nasa.gov/PRODOCS/narsto/table_narsto.html from Langley DAAC, Hampton, Virginia, 2002). Isoprene, MVK, and MACR were determined using the same autosampler used for the PROPHET study, except that the sample volumes were much larger (3.0 L compared to 0.3 L) leading to much lower detection limits. Formaldehyde concentrations were estimated to be 2 ppb [*Cantrell et al.*, 1992; *Apel et al.*, 1998]. As for Kejimkujik, [acetaldehyde] was estimated to be 20% of formaldehyde, or 0.4 ppb.

[23] For CFA, ozone was determined using a UV absorbance method (NOAA), as described by *Ridley et al.* [1992]. NO_x was determined using ozone chemiluminescence [*Williams et al.*, 1998]. Isoprene, MVK, MACR, and

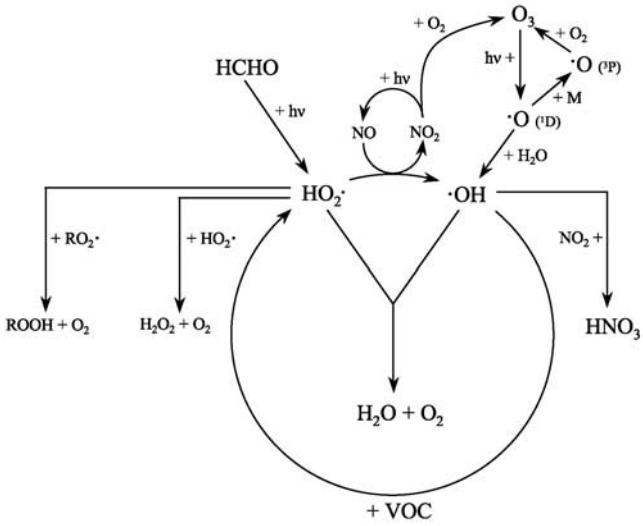

Figure 3. HO_x chemistry reaction scheme.

acetaldehyde were determined using solid sorbent preconcentration, cryofocusing, and GC/FID detection as described by *Stroud et al.* [2001]. Measurements of HCHO were conducted (data courtesy of NCAR) using tunable diode laser absorption spectroscopy, as described by *Fried et al.* [1998]. OH measurements were performed by Pennsylvania State University, and the details of the methodology and data are provided by *Martinez et al.* [2003].

3. Steady State HO_x Calculation

3.1. Derivation of Steady State Expression

[24] Since HO_x data were available at only two of the ground sites, it was necessary to estimate $[HO_x]$ using the assembled measurement data. During the daytime, the steady state approximation can be applied to HO_x, as the lifetime of HO_x (~100 s under daytime Dickson conditions) is short compared to the timescale for significant change in its rate of production or destruction. Therefore we can expand equation (5) to provide an analytical

$$d[HO_x]/dt = 0 = P_{HOx} - L_{HOx} \quad (5)$$

solution. P_{HOx} and L_{HOx} are overall production and loss terms, respectively. The calculation is based on a 10-reaction sequence composed of the dominant reactions that influence tropospheric HO_x [*Crutzen*, 1974; *Logan et al.*, 1981; *Perner et al.*, 1987; *Mount and Williams*, 1997]. Figure 3 is a reaction scheme that depicts all of the reactions used in the steady state calculation. The reactions and rate constants used for the calculation are listed in Table 2.

[25] To apply the calculated [OH] to the MVK and isoprene data sets, we used the following limitations and assumptions: (1) Only data from 1000 to 1600 local time were used to ensure the steady state assumption for HO_x was valid; (2) the concentration of organic peroxy radicals $[RO_2]$ equals that of $[HO_2]$ radicals for midday conditions [*Stockwell et al.*, 1990]; (3) each VOC oxidation yields one HO_2; (4) the production of HO_2 (R_{13a} + $2R_{14}$) equals the rate of destruction of HO_2 via R_6. A calculation assuming a concentration of 1.0×10^6 molecules/cm^3 for [OH] and 1.0×10^8 molecules/cm^3 for $[HO_2]$ and $[RO_2]$ shows that when NO = 50 ppt, 85% of the HO_2 radicals and 87% of the RO_2 radicals react with NO. For all sites the NO concentrations were above 50 ppt for the entire study; therefore assumption 4 is a good approximation.

[26] It is assumed that the important HO_x initiation steps are the photolysis of both ozone and formaldehyde [*Thornton*

Table 2. Reactions and Corresponding Rate Constants Used in the Steady State Calculations

	Number	Rate Constant[a]	Reference
Reactions			
$O_3 + hv \rightarrow O(^1D) + O_2$	(R8)	varying J values	see text
$O(^1D) + H_2O \rightarrow 2\ OH$	(R9)	2.2×10^{-10}	*Sander et al.* [2000]
$O(^1D) + M \rightarrow O(^3P)$	(R10)	2.9×10^{-11}	*DeMore et al.* [1997]
$OH + NO_2 \rightarrow HNO_3$	(R7)	9.0×10^{-12}	*Sander et al.* [2000]
$HO_2 + HO_2 \rightarrow H_2O_2 + O_2$	(R11)	6.1×10^{-12}	*DeMore et al.* [1997]
$HO_2 + RO_2 \rightarrow ROOH + O_2$	(R3)	1.3×10^{-11}	estimated from *Kirchner and Stockwell* [1996]
$OH + HO_2 \rightarrow H_2O + O_2$	(R12)	1.1×10^{-10}	*Sander et al.* [2000]
$OH + VOC \rightarrow HO_2$	(R13a)	see below	see below
$HO_2 + NO \rightarrow OH + NO_2$	(R6)	8.1×10^{-12}	*DeMore et al.* [1997]
$HCHO + hv \rightarrow 2HO_2 + CO$	(R14)	varying J values	see text
OH + isoprene	(R13b)	1.10×10^{-10}	*Stevens et al.* [1999]
OH + MVK	(R13c)	1.88×10^{-11}	*Atkinson* [1994]
OH + MACR	(R13d)	3.35×10^{-11}	*Atkinson* [1994]
OH + HCHO	(R13e)	9.20×10^{-12}	*Atkinson et al.* [1999]
OH + acetaldehyde	(R13f)	1.58×10^{-11}	*Atkinson* [1994]
$OH + CH_4$	(R13g)	6.40×10^{-15}	*Atkinson et al.* [1999]
OH + CO	(R13h)	2.4×10^{-13}	*DeMore et al.* [1997]
$OH + H_2$	(R13i)	6.7×10^{-15}	*DeMore et al.* [1997]

[a]Units are cm^3 molecules^{-1} s^{-1}, estimated for 298 K, 760 torr.

et al., 2002]. Total HO_x production is the sum of the initiation steps as represented in equation (6).

$$P_{HOx} = \frac{2J_8[O_3]}{(1 + k_{10}[M]/k_9[H_2O])} + 2J_{14}[HCHO] \quad (6)$$

J_{14} represents the radical generating pathway from HCHO photolysis. The radical termination steps are represented in reactions (R7), (R11), (R3), and (R12). Therefore the total rate of HO_x loss, L_{HOx}, is represented in equation (7).

$$L_{HOx} = k_7[OH][NO_2] + 2k_{11}[HO_2]^2 + 2k_3[RO_2][HO_2] + 2k_{12}[OH][HO_2] \quad (7)$$

[27] To write equation (7) only in terms of OH, we assume that the rate of HO_2 production from reactions (R13a) and (R14) equals the destruction of HO_2 via reaction (R6). This assumption leads to equation (8).

$$2J_{14}[HCHO] + k_{13a}[VOC][OH] = k_6[HO_2][NO] \quad (8)$$

[28] Equation (8) can be rearranged to give equation (9).

$$[HO_2] = (2J_{14}[HCHO] + k_{13a}[VOC][OH])/k_6[NO] \quad (9)$$

[29] We now substitute equation (9) into equation (7), which removes the $[HO_2]$ term. Finally, we substitute equations (6) and (7) into equation (5), subsequently factoring out the OH and multiplying through by -1 to produce equation (10).

$$\begin{aligned} -d[HO_x]/dt = 0 = {} & \left\{((2k_{11} + 2k_3)\left(k_{13a}^2[VOC]^2/k_6^2[NO]^2\right) \right. \\ & \left. + (2k_{12}k_{13a}[VOC]/k_6[NO])\right\} \cdot [OH]^2 \\ & + \left\{k_7[NO_2] + \left((2k_{11} + 2k_3)\right.\right. \\ & \left.\left. \cdot 4J_{14}[HCHO]k_{13a}[VOC]/k_6^2[NO]^2\right) \right. \\ & \left. + 4k_{12}J_{14}[HCHO]/k_6[NO]\right\} \cdot [OH] \\ & + \left\{[-2J_8[O_3]/(1 + k_{10}[M]/k_9[H_2O])] \right. \\ & \left. - \left[(2J_{14}[HCHO]) + \left((2k_{11} + 2k_3)\right.\right.\right. \\ & \left.\left.\left. \cdot 4J_{14}^2[HCHO]^2/k_6^2[NO]^2\right)\right]\right\} \end{aligned} \quad (10)$$

Equation (10) is in a form that can be solved for OH using the quadratic equation, as shown in equation (11)

$$[OH] = \frac{-b \pm \left(b^2 - 4ac\right)^{1/2}}{2a} \quad (11)$$

The parameters a, b, and c are provided in equations (12), (13), and (14), respectively.

$$a = (2k_{11} + 2k_3) \cdot \frac{k_{13a}^2[VOC]^2}{k_6^2[NO]^2} + \frac{2k_{12}k_{13a}[VOC]}{k_6[NO]} \quad (12)$$

$$b = k_7[NO_2] + \frac{(2k_{11} + 2k_3) \cdot 4J_{14}[HCHO]k_{13a}[VOC]}{k_6^2[NO]^2} + \frac{4k_{12}J_{14}[HCHO]}{k_6[NO]} \quad (13)$$

$$c = \frac{-2J_8[O_3]}{1 + (k_{10}[M]/k_9[H_2O])} - (2J_{14}[HCHO]) + \frac{(2k_{11} + 2k_3) \cdot 4J_{14}^2[HCHO]^2}{k_6^2[NO]^2} \quad (14)$$

Measurement data for ozone, VOCs, NO, NO_2, HCHO, H_2O, and the measured temperature and pressure were used as inputs to solve for OH concentrations.

3.2. Photolysis Rate Coefficients for Ozone and Formaldehyde

[30] The HO_x calculation used varying photodissociation rate coefficients (J values) for ozone and formaldehyde. J values for Cornelia Fort Air Park were provided by NCAR (R. Shetter, private communication, 2002), while the J values at PROPHET were provided by Desert Research Institute (B. Stockwell, private communication, 2002). The J value data set at PROPHET included data every 30 min; therefore it was necessary to expand the J value data coverage so a more complete time-matched data set was available. The PROPHET J values were expanded from the calculated values by defining a linear function relating radiation measurements, taken at the top of the PROPHET sampling tower, to the calculated J values. Subsequently, the radiation data were fit to the function to produce J values with a 1 min data frequency.

[31] Because J values were not explicitly calculated for Dickson or Kejimkujik, the data from CFA and PROPHET were used to calculate the J values at Dickson and Kejimkujik. For the Dickson site, J values were assumed to be equivalent to those at CFA (50 km to the east) for clear sky conditions, and then scaled as a linear function of the Dickson radiometer data. For J_{O3} and J_{HCHO} at Kejimkujik, the calculated J values from PROPHET (J_P) were scaled according to cos(solar zenith angle) for clear sky conditions, and assuming the same O_3 column density. Data used in this paper from Kejimkujik only included data taken during clear sky days.

3.3. Estimates of HO_2

[32] To calculate HO_2 and RO_2 so that γ can be calculated, we assume that $HO_2 = RO_2$, and that HO_2 and OH are in steady state. Following *Stevens et al.* [1997], the HO_2/OH ratio can be calculated by applying the steady state approximation to HO_x, determined by equating the rates of the reactions that interconvert HO_2 and OH. Here the rate of VOC oxidation, which converts OH into HO_2, is equated with the rate of destruction via HO_2 reaction with NO and O_3. Thus we can calculate the HO_2/OH ratio under steady state conditions, given the available species concentration data, as shown in equation (15):

$$[HO_2]/[OH] = \frac{k_{OH}[Isoprene] + k_{OH}[MVK] + k_{OH}[MACR] + k_{OH}[HCHO] + k_{OH+CH3CHO}0.2[HCHO]}{k_{HO2}[NO] + k_{HO2}[O_3]} \quad (15)$$

[33] Here we take the HCHO and CH_3CHO concentrations as described in the text below, and assume, on the basis of the work of *Sumner et al.* [2001] and *Hurst et al.* [2003] that the 5 VOC species in the numerator represent all

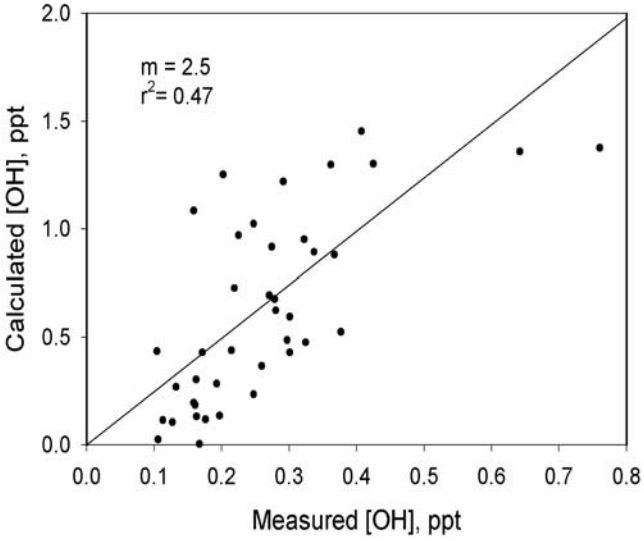

Figure 4. Calculated [OH] versus measured [OH] at Cornelia Fort Airport.

of the VOC-OH reactivity. For each time-matched data point for all sites, we calculate this ratio, given the available measurement data for O_3, NO, and the VOCs. This calculation takes into account the known decrease of HO_2/OH with NO, as discussed by *Stevens et al.* [1997] and *Martinez et al.* [2003]. A detailed discussion of the observed HO_2/OH ratios is provided by *Stevens et al.* [1997], *Tan et al.* [2001], and *Thornton et al.* [2002]. For the four sites studied here the median calculated HO_2/OH ratio and the median observed NO concentration were 401 and 42 ppt for Kejimkujik, 637 and 51 ppt for PROPHET, 143 and 200 ppt for Dickson, and 43 and 422 ppt for CFA.

3.4. Steady State Approximation Output

[34] In Figure 4 we show a plot of time-matched calculated [OH] versus measured ground site [OH] data from the Cornelia Fort Air Park. As shown in Figure 4, the two sets of data are reasonably correlated, but the calculated OH exceeds the measured data by a factor of 2.5. This is not entirely unexpected, as a number of model/measurement comparisons show that [OH] is typically overpredicted [*Eisele et al.*, 1994, 1997; *McKeen et al.*, 1997; *Carslaw et al.*, 1999]. The overestimation of OH by models compared to measurements for these studies ranged from a factor of 4 for *Eisele et al.* [1994] to 1.5 for *McKeen et al.* [1997]. In the *Thornton et al.* [2002] study for Cornelia Fort Airport, it was necessary to increase [CO] (used as a surrogate for VOCs) to 4.5 ppm to make the apparent VOC reactivity consistent with the measurement data. A possible explanation for this overprediction is that OH sinks may be under represented. Specifically, the sum of CO, methane, isoprene, methyl vinyl ketone, HCHO, and acetaldehyde typically make up greater than 85% of the measured reactive hydrocarbon budget in the boundary layer [*Cantrell et al.*, 1993; *Starn et al.*, 1998; *Hurst et al.*, 2003]. However, recent studies indicate that much of the reactive hydrocarbon budget is poorly accounted for using conventional chromatographic sampling and detection schemes. *Lewis et al.* [2000] showed that when standard GC/FID techniques are used, 60% of the carbon balance falls in the C_2-C_6 fraction. However, when comprehensive 2-D GC/FID is used, the C_2-C_6 fraction drops to 20%, while the majority of carbon is found in larger molecules, in the C_6-C_{12} range. Also, in their study of urban air from Melbourne, Australia, 85% of all oxygenated material fell in the C_9-C_{11} range. C_9-C_{11} species are rarely quantified and were not measured at CFA, PROPHET, and Kejimkujik. This observation supports the hypothesis of *McKeen et al.* [1997] that discrepancies between modeled and measured OH values can be attributed to unmeasured hydrocarbon species. This position is further supported from total OH reactivity measurements at CFA [*Kovacs and Brune*, 2001]. The Kovacs study revealed that the measured reactive species (CO, CH_4, formaldehyde, acetaldehyde, isoprene, MVK, and MACR) represent only ~60% of the OH reactivity during daytime, in an environment where most of the measured reactive VOCs were anthropogenic and relatively easy to quantify. Although this fraction increased in the evening, this was reportedly due mainly to increased NO_2 as the boundary layer height decreased in the late afternoon. It is likely that at the other sites, the fraction of the reactivity accounted for was smaller, as the anthropogenic VOCs are less important. On the basis of this analysis we have constrained this steady state model by doubling the measured VOC reactivity. The doubled k_{OH}[VOC] falls within the uncertainty of the determination of the fraction of the reactivity accounted for during the *Kovacs and Brune* [2001] (SOS99) study. A comparison of calculated [OH] (with doubled VOC reactivity) and the actual OH measurement data is presented in Figure 5. For this case, the steady state approximation overpredicts the measurement data by only 1.6. The discrepancy between the calculated values and the measurement data, if significant, may be caused by an underrepresentation of the HO_x sinks described in equation (7). Also, there may be systematic errors in the OH measurement data. In our treatment, a likely significant oversimplification in the calculation is the neglect of the importance of the $RO_2 + NO \rightarrow RONO_2$ reaction as a radical sink under low-[NO_x] conditions [*Thornton et al.*, 2002; *Chen et al.*, 1998]. However, the calculated [OH] are

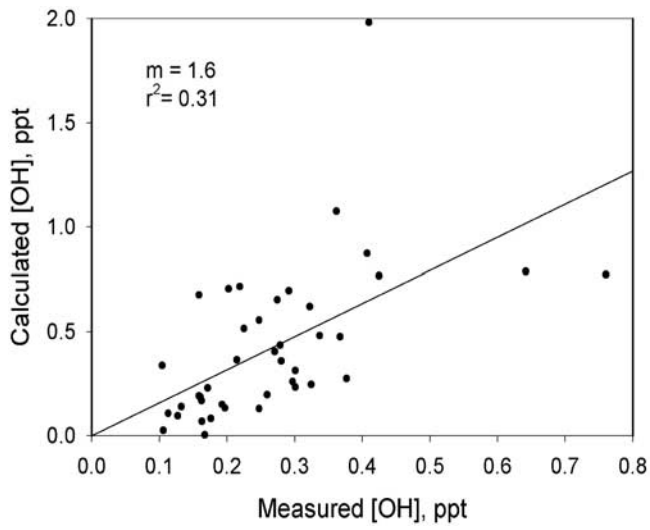

Figure 5. Calculated [OH] with doubled VOC reactivity versus measured [OH] at Cornelia Fort Air Park.

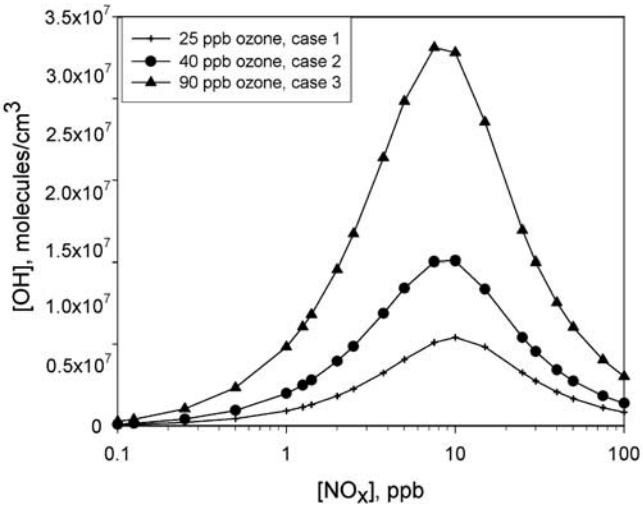

Figure 6. Calculated [OH] versus [NO_x] for different reactant conditions.

within the measurement uncertainties, and thus will provide an acceptable estimate of NO_x-dependent [OH]. We use these doubled-VOC calculated [OH] values here and in the companion study of the NO_x dependence of the production of isoprene nitrates [*Grossenbacher et al.*, 2004].

[35] We note that models do not always overpredict OH; a case in point is the *Martinez et al.* [2003] study, in which OH is underestimated for Cornelia Fort. If in that study, the reactive VOCs were increased to more closely approximate the actual reactivity, the difference between measured and simulated OH would have increased.

[36] To evaluate the general features of the steady state calculation, typical concentrations of pertinent species were input into equation (10). We calculated [OH] as a function of varying [NO_x] while holding other inputs constant, for case studies representative of the four field sites. Parameters that were held constant for all trials were CO, 150 ppb; methane, 1720 ppb; H_2, 500 ppb; and pressure at 760 torr. Case 1, which was typical of values observed at Kejimkujik, comprised the following concentrations: 25 ppb O_3, RH = 60%, 21°C, 4 ppb isoprene, and 2 ppb HCHO. The model conditions for case 2, typical for PROPHET and Dickson, were: 40 ppb O_3, RH = 80%, 26.5°C, 2 ppb isoprene, and 3 ppb HCHO. Case 3, typical for CFA, was run with the following conditions: 90 ppb O_3, RH = 75%, 32°C, 1 ppb isoprene, and 4 ppb HCHO. The results for each case as a function of [NO_x] (for t = 1200) are shown in Figure 6. The overall shape of the relationship between OH and NO_x is as predicted by *Weinstock et al.* [1981] and shown in box models by *Lin et al.* [1988], *Trainer et al.* [1987], and *McKeen et al.* [1997]. As shown in Figure 6, when NO_x is high, OH is suppressed because of HNO_3 production in reaction (R7). At low NO_x, HO_x radicals terminate via self-reaction and reactions with RO_2 (reactions (R11) and (R3)). Note that the OH concentration maximizes at NO_x concentrations corresponding to 6–10 ppb NO_x.

4. Results and Discussion

4.1. Calculated OH for All Field Sites

[37] All daytime measurement data from all four field sites were used to generate a plot of calculated OH versus observed NO_x, shown in Figure 7. The calculated OH was binned into increments of NO_x that were equidistant on a log scale and subsequently averaged. The horizontal bars represent the bin width, and the vertical error bars represent one standard deviation of the average for each bin. Note that the four study sites cover a range of NO_x concentrations from 50 ppt to 30 ppb. Over that range, calculated [OH] varies from 2.6×10^4 molecules/cm^3 to 4.9×10^7 molecules/cm^3. While the data set has large variability, as shown by the error bars, the binned average data display an OH profile that is indicative of the functional form of OH as a function of NO_x. The bins that correspond to the highest calculated OH concentrations are 3.2–5.6, 5.6–10.0, and 10.0–17.8 ppb NO_x. These correspond to typical conditions prevailing at the CFA site. Figure 7 also shows the CFA measurement data used for Figures 4 and 5, binned and averaged as for the calculated OH values. The photochemical box model study discussed by *Lin et al.* [1988] generates an OH profile as a function of [NO_x] that has a similar profile to that in Figure 7, with a maximum OH concentration at 3–4 ppb NO_x. While the Lin et al. model generates a peak OH concentration of 1×10^7 molecules/cm^3, the peak OH concentration, on average, for this model is 1.4×10^7. The [NO_x] range represented here covers most conditions in eastern North America, except for relatively polluted urban conditions.

4.2. Isoprene Oxidation Rate as a Function of NO_x

[38] As described in section 1.2, γ (the fraction of the time that organic peroxy radicals react with NO) is an important variable in the NO_x dependence of the isoprene-OH oxidation. In Figure 8, calculated values for γ (given calculated radical concentrations, and measured [NO]; note that RO_2 is obtained from calculated HO_2, and the assumption that [RO_2] = [HO_2]) are plotted as a function of [NO] for all four sites. As shown in the figure, γ ranges from a minimum of ~0.56 to a maximum of 1.0, at high [NO]. As the NO concentration increases, γ approaches unity. Although one might expect γ to approach 0 as the NO concentration approaches 0, as [NO] decreases so does [OH] as well as [HO_2], and the rates of reactions (R11) and (R3) scale as [HO_2]^2. Thus γ decreases slowly as NO_x approaches 0.05 ppb.

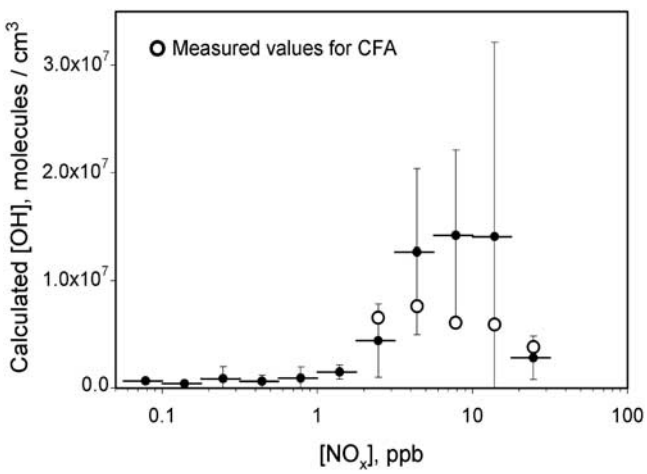

Figure 7. Binned averages of calculated [OH] for all sites versus observed [NO_x].

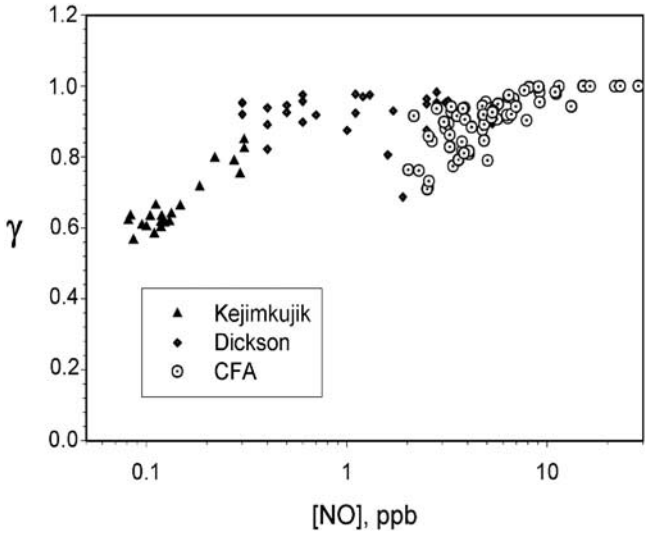

Figure 8. The γ versus observed [NO] for Kejimkujik, Dickson, and CFA.

[39] Given γ, it is possible to calculate the MVK production rates via equation (3), using the observed [isoprene] and [NO], and calculated [OH] data. We note that this ignores MVK production from isoprene ozonolysis; however, during daytime conditions, OH reaction with isoprene is about 2 orders of magnitude faster than is ozonolysis. Figure 9 depicts the calculated instantaneous MVK production rate for all four field sites as a function of [NO_x]. Although there is not a large difference in daytime [isoprene] among the four sites, there is a large range of MVK production rates, because of the NO_x dependence of OH and γ. As expected, the calculated MVK production rate follows the OH profile, with a maximum in P[MVK] in the 4–6 ppb NO_x range.

[40] As indicated from equation (4), P[MVK]/[isoprene] should correlate with $[OH]\{(\gamma \cdot \alpha) + (1 - \gamma) \cdot \beta)\}$. Figure 10a shows the calculated $[OH]\{(\gamma \cdot \alpha) + (1 - \gamma) \cdot \beta)\}$ versus observed [NO_x] from the Kejimkujik, Dickson, and CFA sites. Figure 10b shows the observed [MVK]/[isoprene] ratio versus observed [NO_x] from these same field sites. MVK data from PROPHET was not used in this analysis, as the data quality was relatively poor, and as *Apel et al.* [2002] have discussed, because the manifold inlet is situated ~12 m above the canopy, isoprene is relatively unprocessed, yielding unusually small [MVK]/[isoprene] ratios. For CFA, Kejimkujik, and Dickson, the inlets are in a clearing, and we thus expect relatively longer (but comparable) effective reaction times, e.g., as discussed by *Stroud et al.* [2001]. The bin widths in Figure 10 are equidistant on a log scale and are depicted by the horizontal bars. The vertical bars show 1 standard deviation from the average value in the bin. As with previous calculations and plots, all data are time matched and taken from 1000 to 1600 local time. As shown the calculated $[OH]\{(\gamma \cdot \alpha) + (1 - \gamma) \cdot \beta)\}$ term peaks at 5.6–17.8 ppb NO_x, consistent with the observed and independent [MVK]/[isoprene] ratio, which also peaks at ~5.6–17.8 ppb NO_x. The shapes of the calculated (Figure 10a) and measured (Figure 10b) profiles are quite similar. This represents the first comprehensive determination of the NO_x dependence of OH chemistry through the measurement of a VOC oxidation product. Note that while the ordinate in Figure 10a is equal to P[MVK]/[isoprene], we have plotted [MVK]/[isoprene] in Figure 10b. The implicit assumption is that for each condition [MVK] $\propto$ d[MVK]/dt; in other words, we are effectively assuming either a comparable NO_x dependence of the MVK loss rates or that the rate of MVK production is much greater than the MVK loss rate, which is generally the case for daytime hours, as discussed above. The observation in Figure 10b is significant, in that it confirms the crossover between NO_x-limited and VOC-limited conditions at ~10 ppb NO_x

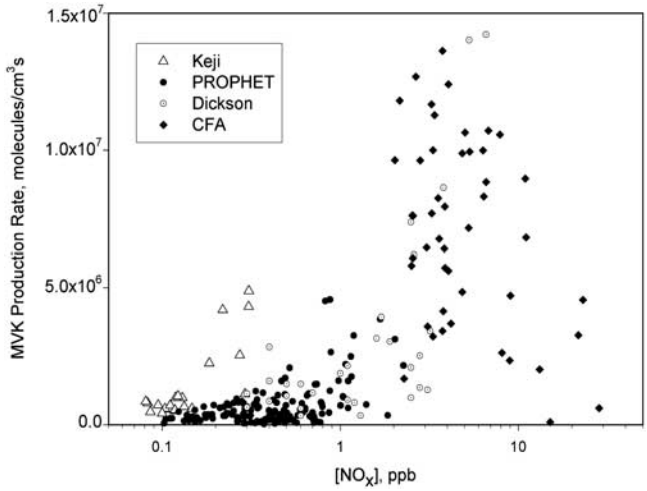

Figure 9. Calculated MVK production rates versus observed [NO_x] from all four field sites.

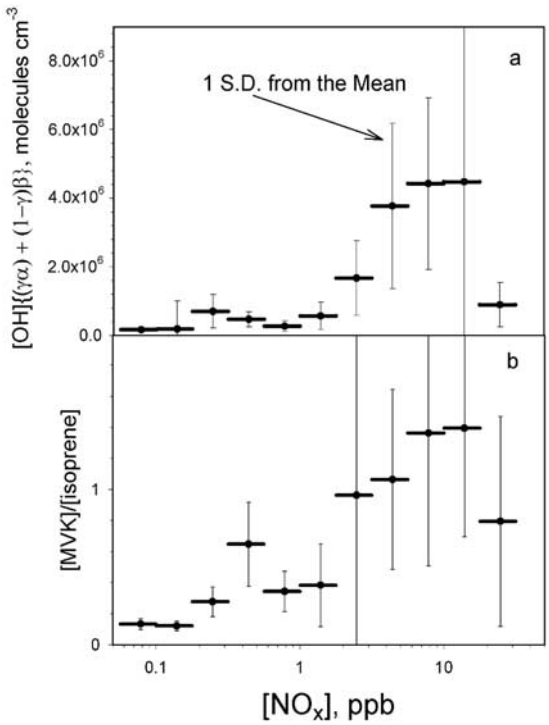

Figure 10. (a) NO_x-dependent MVK production variables and (b) [MVK]/[isoprene] versus observed [NO_x].

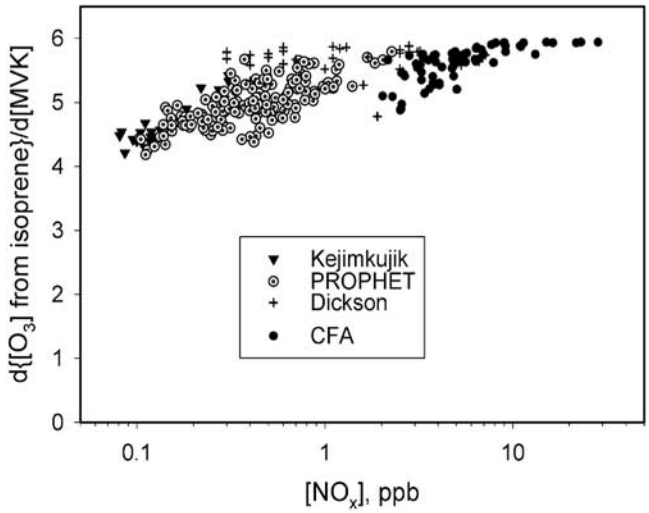

Figure 11. Ozone generated per MVK versus observed $[NO_x]$.

[cf. *Frost et al.*, 1998; *Thornton et al.*, 2002], as has been inferred from calculations of the ozone production rate versus NO_x. We note that that part of Figure 10 derives essentially only from CFA and Dickson data, as the Kejimkujik site does not exhibit NO_x levels that high. Although the [OH] calculation used here carries a number of simplifying assumptions, the agreement in the crossover from the calculated [OH] and the independently determined [MVK]/[isoprene] ratio supports the conclusion of a ~10 ppb crossover point, at least in the eastern North America environment represented by the Dickson/CFA sites.

4.3. Ozone Production From Isoprene Oxidation

[41] As discussed in section 1.1, we can estimate the amount of ozone produced for each isoprene oxidized, making use of the MVK and O_3 data. To do so properly, we need to consider γ, the fraction of isoprene peroxy radicals that react with NO, as shown in equation (16).

$$P(O_3 \text{ from Isoprene}) = 2 \cdot 0.956 \cdot R1 \cdot \gamma = 1.91 \cdot R1 \cdot \gamma \quad (16)$$

Equation (17) provides a solution to d(O_3 from isoprene)/d(MVK) as follows:

$$\frac{P(O_3 \text{ from Isoprene})}{P[MVK]} = \frac{1.91 \cdot \cancel{R1} \cdot \gamma}{\cancel{R1}\{(\gamma \cdot \alpha) + (1-\gamma)\beta)\}} = \frac{1.91\gamma}{(\gamma \cdot \alpha) + (1-\gamma) \cdot \beta} \quad (17)$$

The right side of equation (17) is plotted against observed $[NO_x]$ in Figure 11, making use of our calculated values for γ. The range of ozone molecules produced (from isoprene oxidation) as a function of [MVK] covers a relatively small range, i.e., from ~4.2 to 6.0 ozone molecules per MVK. We note that the range of isoprene nitrate yields in the literature is from 4.4 to 13%, the latter being the upper limit reported by *Tuazon and Atkinson* [1990]. If that value is utilized, the numerator on the right side of equation (17) becomes 1.74γ, and the high-NO_x limit (when $\gamma = 1$) would correspond to a value of 5.4O_3 per MVK, rather than 6.0. This provides a very useful means for determining the contribution of isoprene chemistry to ozone production using atmospheric MVK measurements. The number of ozone molecules produced from isoprene per MVK molecule is relatively invariant to NO_x (because of the small NO_x dependence of γ, as discussed above); therefore, as MVK measurements are available the contribution to ozone production can be estimated for a wide range of $[NO_x]$. As shown in Figure 11, the upper limit of P(O_3 from isoprene)/MVK approaches 6.0 as $\gamma \rightarrow 1$, as indicated from equation (1) (i.e., since α = 0.32).

[42] Given [OH] and γ, and our isoprene data, we can calculate the rate of O_3 production as derived from isoprene oxidation in this environment as a function of $[NO_x]$, as shown in equation (18). Figure 12 shows the calculated ozone production rate from isoprene in units of

$$P(O_3 \text{ from isoprene}) = k_8[OH][\text{isoprene}] \cdot 1.91 \cdot \gamma \quad (18)$$

ppb per hour from equation (18) plotted versus observed $[NO_x]$, for these same four eastern North American sites, i.e., using the measured [isoprene] data. Data were used from all four field sites to calculate [OH] and γ. The bin widths are equidistant on a log scale and are depicted by the horizontal bars. The vertical bars show 1 standard deviation from the average value in the bin. The data indicate a substantial increase in ozone production from isoprene between 0.1 ppb and 10 ppb NO_x. At sufficiently high $[NO_x]$, O_3 production from isoprene begins to decrease, corresponding to a decrease in [OH]. As shown in Figure 12, the daytime boundary layer O_3 production rates vary from 1 to 5 ppb ozone per hour on average, similar to those reported by *Chameides et al.* [1992] for rural sites in the eastern United States, implying that, for moderate NO_x concentrations, isoprene chemistry produces a significant fraction of the observed ozone in summer (consistent with the discussion in section 1.1). *Thornton et al.* [2002] calculate a total O_3 production rate of 25 ppb/h for $[NO_x]$ =

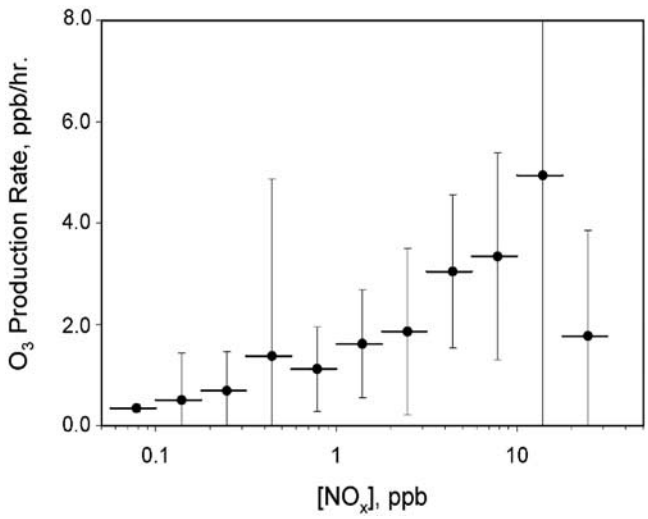

Figure 12. Ozone production rate from isoprene-OH oxidation versus observed $[NO_x]$.

4–5 ppb for CFA. This indicates an isoprene contribution to O_3 production of approximately 15% for these conditions in the urban environment near CFA, on average.

5. Conclusions

[43] The MVK/isoprene data for a wide range of NO_x conditions exhibit a NO_x dependence that is very similar to the NO_x dependence of the calculated [OH], and these are both consistent with previous models and HO_x measurement data. The crossover between NO_x- and VOC-limited conditions ($\sim$10 ppb NO_x), revealed in this analysis, is consistent with that observed from direct HO_x measurement data. We have shown here that the rate of isoprene oxidation at various North American sites is highly variable, with a NO_x dependence that peaks at $\sim$8 ppb [NO_x].

[44] This work also reveals the impact varying [NO_x] can have on BVOC oxidation, and in turn, ozone production from BVOC oxidation, as well as nitrogen sequestration via BVOC oxidation [*Grossenbacher et al.*, 2004]. Isoprene oxidation results in the largest ozone production rates for NO_x concentrations in the range of $\sim$1–10 ppb. This NO_x concentration range is representative of conditions corresponding to relatively anthropogenically impacted rural environments. The results clearly show the large impact that urban emissions and power plant plumes may have on initiating isoprene chemistry in downwind forest environments.

[45] **Acknowledgments.** We would like to acknowledge the NASA Earth System Science Fellowship grant NGT5-30163, the United States EPA via grant R825256-01-0, and NOAA for their support during the Southern Oxidant Study 1999. We are grateful to the University of Michigan Biological Station for the use of their excellent facilities and archived data. We thank Rick Shetter of NCAR for providing CFA $J(O_3)$ and J(HCHO) data and Bill Stockwell of DRI for PROPHET $J(O_3)$ and J(HCHO). We are grateful to William Brune, Monica Martinez, and Hartwig Harder of Pennsylvania State University for access to OH data at Cornelia Fort Airport and for helpful editorial comments on this manuscript. We acknowledge Ian Faloona of University of California, Davis, for useful comments and recommendations relative to this work.

References

Apel, E., et al. (1998), Measurement comparison of oxygenated volatile organic compounds at a rural site during the 1995 SOS Nashville Intensive, *J. Geophys. Res.*, *103*, 22,295–22,316.

Apel, E. C., et al. (2002), Measurement and interpretation of isoprene fluxes and isoprene, methacrolein, and methyl vinyl ketone mixing ratios at the PROPHET site during the 1998 intensive, *J. Geophys. Res.*, *107*(D3), 4034, doi:10.1029/2000JD000225.

Atkinson, R. (1994), Gas-phase tropospheric chemistry of organic compounds, *J. Phys. Chem. Ref. Data Monogr.*, *2*, 216 pp.

Atkinson, R., D. Baulch, R. Cox, R. Hampson, J. Kerr, M. Rossi, and J. Troe (1999), Evaluated kinetic and photochemical data for atmospheric chemistry, organic species: Supplement VII, *J. Phys. Chem. Ref. Data*, *28*, 215–288.

Barket, D. J., Jr., et al. (2001), Intercomparison of automated methodologies for measurement of ambient isoprene during PROPHET 1998 summer campaign, *J. Geophys. Res.*, *106*, 24,301–24,313.

Biesenthal, T., Q. Wu, P. Shepson, H. Wiebe, K. Anlauf, and G. Mackay (1997), A study of relationships between isoprene, its oxidation products, and ozone, in the lower Fraser Valley, BC, *Atmos. Environ.*, *31*, 2049–2058.

Biesenthal, T., J. Bottenheim, P. Shepson, S.-M. Li, and P. Brickell (1998), The chemistry of biogenic hydrocarbon at a rural site in eastern Canada, *J. Geophys. Res.*, *103*, 25,487–25,498.

Bottenheim, J., A. Sirois, K. Brice, and A. Gallant (1994), Five years of continuous observations of PAN and ozone at a rural location in eastern Canada, *J. Geophys. Res.*, *99*, 5333–5352.

Cantrell, C., et al. (1992), Peroxy-radicals in the ROSE experiment: Measurement and theory, *J. Geophys. Res.*, *97*, 20,671–20,686.

Cantrell, C., R. Shetter, and J. Calvert (1993), Peroxy radicals as measured in ROSE and estimated from photostationary state deviations, *J. Geophys. Res.*, *98*, 18,355–18,366.

Carroll, M. A., P. B. Shepson, and S. B. Bertman (2001), Overview of the Program for Research on Oxidants: Photochemistry, Emissions, and Transport (PROPHET) summer 1998 measurements intensive, *J. Geophys. Res.*, *106*, 24,275–24,288.

Carslaw, N., D. Creasy, D. Heard, A. Lewis, P. Monks, B. Brandy, and S. Penkett (1999), Modeling OH, HO_2 and RO_2 radicals in the marine boundry layer: 1. Model construction and comparison with field measurements, *J. Geophys. Res.*, *104*, 30,241–30,255.

Chameides, W., R. Lindsay, J. Richardson, and C. Kiang (1988), The role of biogenic hydrocarbons in urban photochemical smog: Atlanta as a case study, *Science*, *241*, 1473–1475.

Chameides, W. L., F. Fehsenfeld, M. O. Rodgers, C. Cardelino, J. Greenberg, P. Middleton, and T. Wang (1992), Ozone precursor relationship in the ambient atmosphere, *J. Geophys. Res.*, *97*, 6037–6055.

Chen, X., D. Hulbert, and P. Shepson (1998), Measurement of the organic nitrate yield from OH reaction with isoprene, *J. Geophys. Res.*, *103*, 25,563–25,568.

Chin, M., D. J. Jacob, J. W. Munger, D. D. Parrish, and B. G. Doddridge (1994), Relationship of ozone and carbon-monoxide over North America, *J. Geophys. Res.*, *99*, 14,565–14,573.

Cooper, O. R., J. L. Moody, T. Thornberry, M. Town, and M. A. Carroll (2001), PROPHET 1998 meteorological overview and air-mass classification, *J. Geophys. Res.*, *106*, 24,289–24,299.

Crutzen, P. (1974), Photochemical reactions initiated by and influencing ozone in unpolluted tropospheric air, *Tellus*, *26*, 47–57.

DeMore, W. B., S. P. Sander, D. M. Golden, R. F. Hampson, M. J. Kurylo, C. J. Howard, A. R. Ravishankara, C. E. Kolb, and M. J. Molin (1997), Chemical kinetics and photochemical data for use in stratospheric modeling: Evaluation number 12, *JPL Publ.*, *97-4*.

Dlugokencky, E. J., L. P. Steele, P. M. Lang, and K. A. Masarie (1994), The growth rate and distribution of atmospheric methane, *J. Geophys. Res.*, *99*, 17,021–17,043.

Eisele, F., G. Mount, F. Fehsenfeld, J. Harder, E. Marovich, D. Parrish, J. Roberts, M. Trainer, and D. Tanner (1994), Intercomparison of tropospheric OH and ancillary trace gas measurements at Fritz-Peak-Observatory, Colorado, *J. Geophys. Res.*, *99*, 18,605–18,626.

Eisele, F. L., G. H. Mount, D. Tanner, A. Jefferson, R. Shetter, J. W. Harder, and E. J. Williams (1997), Understanding the production and interconversion of the hydroxyl radical during the Tropospheric OH Photochemistry Experiment, *J. Geophys. Res.*, *102*, 6457–6465.

Faloona, I., et al. (2001), Nighttime observations of anomalously high levels of hydroxyl radicals above a deciduous forest canopy, *J. Geophys. Res.*, *106*, 24,315–24,333.

Fried, A., B. Henry, B. Wert, S. Sewell, and J. Drummond (1998), Laboratory, ground-based and airborne tunable diode laser systems: Performance characteristics and applications in atmopheric studies, *Appl. Phys. B*, *67*, 317–330.

Frost, G. J., et al. (1998), Photochemical ozone production in the rural southeastern United States during the 1990 Rural Oxidants in the Southern Environment (ROSE) program, *J. Geophys. Res.*, *103*, 22,491–22,508.

Grossenbacher, J. W., D. J. Barket Jr., P. B. Shepson, M. A. Carroll, K. Olszyna, and E. Apel (2004), A comparison of isoprene nitrate concentrations at two forest-impacted sites, *J. Geophys. Res.*, *109*, D11311, doi:10.1029/2003JD003966.

Guenther, A., et al. (1995), A global model of natural volatile organic compound emissions, *J. Geophys. Res.*, *100*, 8873–8892.

Hurst, J. M., D. J. Barket, and P. B. Shepson (2003), The atmospheric chemistry of nonanal, *Environ. Sci. Technol.*, *37*, 2218–2225.

Jenkin, M. E., A. A. Boyd, and R. Lesclaux (1998), Peroxy radical kinetics resulting from the OH-Initiated oxidation of 1, 3-butadiene, 2, 3-dimethyl-1, 3-butadiene and isoprene, *J. Atmos. Chem.*, *29*, 267–298.

Kirchner, F., and W. Stockwell (1996), Effect of peroxy radical reactions on the predicted concentrations of ozone, nitrogenous compound, and radials, *J. Geophys. Res.*, *101*, 21,007–21,022.

Kovacs, T., and W. Brune (2001), Total OH loss rate measurement, *J. Atmos. Chem.*, *39*, 105–122.

Leaitch, W. R., J. W. Bottenheim, T. A. Biesenthal, S. M. Li, P. S. K. Liu, K. Asalian, H. Dryfhout-Clark, F. Hopper, and F. Brechtel (1999), A case study of gas-to-particle conversion in an eastern Canadian forest, *J. Geophys. Res.*, *104*, 8095–8111.

Lei, W. F., R. Y. Zhang, W. S. McGivern, A. Derecskei-Kovacs, and S. W. North (2001), Theoretical study of OH-O-2-isoprene peroxy radicals, *J. Phys. Chem. A*, *105*, 471–477.

Lewis, A. C., N. Carslaw, P. J. Marriott, R. M. Xinghorn, P. Morrison, A. L. Lee, K. D. Bartle, and M. J. Pilling (2000), A larger pool of ozone-formaing carbon compounds in urban atmospheres, *Nature*, *405*, 778–781.

Lin, X., M. Trainer, and S. C. Liu (1988), On the nonlinearity of the tropospheric ozone production, *J. Geophys. Res.*, *93*, 15,879–15,888.

Logan, J., M. Prather, S. Wofsy, and M. McElroy (1981), Tropospheric chemistry: A global perspective, *J. Geophys. Res.*, *86*, 7210–7254.

Martinez, M., et al. (2003), OH and HO_2 concentrations, sources, and loss rates during the Southern Oxidants Study in Nashville, Tennessee, summer 1999, *J. Geophys. Res.*, *108*(D19), 4617, doi:10.1029/2003JD003551.

McKeen, S. A., et al. (1997), Photochemical modeling of hydroxyl and its relationship to other species during the Tropospheric OH Photochemistry Experiment, *J. Geophys. Res.*, *102*, 6467–6493.

Miyoshi, A., S. Hatakeyama, and N. Washida (1994), OH radical initiated photooxidation of isoprene: An estimate of global CO production, *J. Geophys. Res.*, *99*, 18,779–18,787.

Mount, G. H., and E. J. Williams (1997), An overview of the Tropospheric OH Photochemistry experiment, Fritz Peak/Idaho Hill, Colorado, fall, *J. Geophys. Res.*, *102*, 6171–6186.

Olszyna, K. J., W. J. Parkhurst, and J. F. Meagher (1998), Air chemistry during the 1995 SOS/Nashville intensive determined from level 2 network, *J. Geophys. Res.*, *103*, 31,143–31,153.

Padro, J. (1996), Summary of ozone dry deposition velocity measurements and model estimates over vineyard, cotton, grass, and deciduous forest in summer, *Atmos. Environ.*, *30*, 2363–2369.

Perner, D., et al. (1987), Tropospheric OH concentrations: A comparison of field data with model predictions, *J. Atmos. Chem.*, *5*, 185–216.

Ridley, B. A., S. Madronich, R. B. Chatfield, J. G. Walega, R. E. Shetter, M. A. Carroll, and D. D. Montzka (1992), Measurements and model simulations of the photostationary state during the Mauna Loa Observatory Photochemistry Experiment: Implications for radical concentrations and ozone production and loss rates, *J. Geophys. Res.*, *97*, 10,375–10,388.

Sander, S. P., W. B. DeMore, D. M. Goldan, R. F. Hampson, M. J. Kurylo, C. J. Howard, A. R. Ravishankara, C. E. Kolb, and M. J. Molina (2000), Chemical kinetics and photochemical data for use in atmospheric modeling, *JPL Publ.*, *97-4*.

Shepson, P. B., D. R. Hastie, H. I. Schiff, M. Polizzi, J. W. Bottenheim, K. Anlauf, G. I. Mackay, and D. Karecki (1991), Atmospheric concentrations and temporal variations of C_1–C_3 carbonyl compounds at two rural sites in central Ontario, *Atmos. Environ., Part A*, *25*, 2001–2015.

Starn, T., P. Shepson, S. Bertman, J. White, B. Splawn, D. Riemer, R. Zika, and K. Olszyna (1998), Observations of isoprene chemistry and its role in ozone production at a semirural site during the 1995 Southern Oxidants Study, *J. Geophys. Res.*, *103*, 22,425–22,435.

Stevens, P. S., et al. (1997), HO_2/OH and RO_2/HO_2 ratios during the Tropospheric OH Photochemistry Experiment: Measurement and theory, *J. Geophys. Res.*, *102*, 6379–6392.

Stevens, P., D. L'Esperance, B. Chuong, and G. Martin (1999), Measurements of the kinetics of the OH-initiated oxidation of isoprene: Radical propagation in the OH + isoprene + O_2 + NO reaction system, *Int. J. Chem. Kinet.*, *31*, 637–643.

Stockwell, W. R., P. Middleton, J. S. Chang, and X. Y. Tang (1990), The 2nd Generation Regional Acid Deposition Model Chemical Mechanism For Regional Air Quality Modeling, *J. Geophys. Res.*, *95*, 16,343–16,367.

Stroud, C., et al. (2001), Isoprene and its oxidation products, methacrolein and methylvinyl ketone, at an urban forested site during the 1999 Southern Oxidants Study, *J. Geophys. Res.*, *106*, 8035–8045.

Sumner, A., et al. (2001), A study of the formaldehyde budget above a forest canopy, *J. Geophys. Res.*, *106*, 24,387–24,405.

Tan, D. (2001), HO_x budgets in a deciduous forest: Results from the PROPHET summer 1998 campaign, *J. Geophys. Res.*, *106*, 24,407–24,427.

Thornberry, T., et al. (2001), Observations of reactive oxidized nitrogen and speciation of NO_y during the PROPHET summer 1998 intensive, *J. Geophys. Res.*, *106*, 24,359–24,386.

Thornton, J. A., et al. (2002), Ozone production rates as a function of NO_x abundances and HO_x production rates in the Nashville urban plume, *J. Geophys. Res.*, *107*(D12), 4146, doi:10.1029/2001JD000932.

Trainer, M., E. Y. Hsie, S. A. McKeen, R. Tallamraju, D. D. Parrish, F. C. Fehsenfeld, and S. C. Liu (1987), Impact of natural hydrocarbons on hydroxyl and peroxy radicals at a remote site, *J. Geophys. Res.*, *92*, 11,879–11,894.

Tuazon, E., and R. Atkinson (1990), A product study of the gas-phase reaction of isoprene with the OH radical in the presence of NO_x, *Int. J. Chem. Kinet.*, *22*, 1221–1236.

Weinstock, B., H. Niki, and T. Chang (1981), Chemical factors affecting the hydroxyl radical concentration in the troposphere, *Adv. Environ. Sci. Technol.*, *10*, 221–258.

Williams, E., et al. (1998), Intercomparison of ground-based NO_y measurement techniques, *J. Geophys. Res.*, *103*, 22,261–22,281.

D. J. Barket Jr. and J. W. Grossenbacher, Griffin Analytical Technologies, Inc., 3000 Kent Avenue, West Lafayette, IN 47906, USA. (barket@griffinanalytical.com; grossenbacher@griffinanalytical.com)

T. Biesenthal, Sciex, 71 Four Valley Drive, Concord, Ontario, Canada L4K 4V8. (thomas.biesenthal@nrc.ca)

J. Bottenheim, Meteorological Service of Canada, 4905 Dufferin Street, Downsview, Ontario, Canada M3H 5T4. (jan.bottenheim@ec.gc.ca)

M. A. Carroll and T. Thornberry, Department of Atmospheric, Oceanic, and Space Sciences, University of Michigan, 2455 Hayward Street, Ann Arbor, MI 48109, USA. (mcarroll@umich.edu; tthornbe@chem.utoronto.ca)

J. M. Hurst and P. B. Shepson, Department of Chemistry, Purdue University, 1393 Brown Building, West Lafayette, IN 47907, USA. (juliabowman420@hotmail.com; pshepson@purdue.edu)

K. Olszyna, Atmospheric Sciences Department, Tennessee Valley Authority, CEB 2A, Muscle Shoals, AL 35662, USA. (kjolszyna@tva.gov)

J. Roberts and C. Stroud, NOAA Aeronomy Laboratory, 325 Broadway, Boulder, CO 80303, USA. (james.m.roberts@noaa.gov; cstroud@acd.ucar.edu)